Bio-inspired heterogeneous Fe_4S_4 single-cluster catalyst for enhanced electrochemical CO_2 reduction to CH_4

Hengyue Xu[1] and Lan Ma[1,2,*]

[1]Institute of Biopharmaceutical and Health Engineering, Tsinghua Shenzhen International Graduate School, Tsinghua University, Shenzhen 518055, China.

[2]Institute of Biomedical Health Technology and Engineering, Shenzhen Bay Laboratory, Shenzhen 518055, China.

Corresponding authors:

Lan Ma, Email: malan@sz.tsinghua.edu.cn

ORCID iD: https://orcid.org/0000-0002-6610-5871

ABSTRACT GRAPHIC

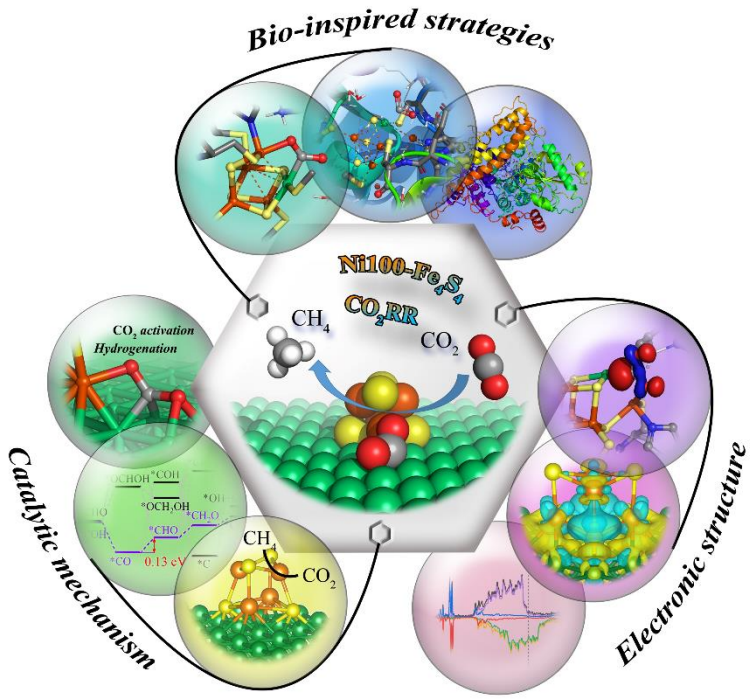

ABSTRACT

Electrochemical conversion of carbon dioxide promises next-level paradigm shifts in sustainability. Applications will include breakthrough solutions to global crisis threatening our civilization, including energy, food, and climate change. Here, inspired by CO dehydrogenase II from *Carboxyothermus hydrogenoformans*, we designed a heterogeneous Fe_4S_4 single-cluster catalyst Ni100-Fe_4S_4, achieving high performance CO_2 electroreduction. Combined with the experimental data and theoretical calculation, Ni100-Fe_4S_4 and CO dehydrogenase have highly similar catalytic geometric centers and CO_2 binding modes. By exploring the origin of catalytic activity of this biomimetic structure, we found the activation of CO_2 by Ni100-Fe_4S_4 theoretically exceeds that of natural CO dehydrogenase. Density functional theory calculations reveal that the dehydrogenase enzyme-liked Fe-Ni active site as an electron enrichment 'electro-bridge', activating CO_2 molecules efficiently and stabilizing various intermediates in multistep elementary reactions to produce CH_4 in a low overpotential (0.13eV) selectively. The calculated electroreduction pathway can completely consistent with the nickel-based catalytic materials reported in the current experiments. This work demonstrates that it is efficient and feasible to design biomimetic high-performance catalytic materials by using blueprints provide by nature. Combining ideas from modern catalyst design with bio-inspired strategies will lead our catalysts beyond its current limitations.

■ INTRODUCTION

Global energy environmental crisis is particularly prominent in the 21st century. The

excessive consumption of fossil fuels has not only brought about a thorny energy crisis, but also could cause global warming[1], abnormal water circulation[2], climate deterioration[3], and extinction of biological populations[4] due to excessive CO_2 emissions. Developing a carbon-neutral strategy provides a path to a bright future for human civilization and the entire planet's biosphere. Electrochemical CO_2 reduction (CO_2RR) to useful fuels and value-added chemical feedstocks while mitigating CO_2 emissions from human activity offers great promise for carbon-neutral strategy. However, the fast and efficient design of low-cost, high activity, high selectivity CO_2 electrocatalysts remains a significant challenge[5,6]. High-throughput random screening and a large number of synthetic tests can indeed find some highly active catalysts[7-9], but it relies on a large number of databases and still consumes huge computing resources, manpower and material resources. Therefore, it is urgent to find a new method to rationally design the electrocatalyst for CO_2 reduction. As one of the efficient, rapid and rational design of catalysts, bionics has been gradually applied to the design of various catalysts in recent years[10-15]. It is fascinating and promising to search for highly active biological carbon-fixing enzymes from the treasure house of microorganisms related to the evolutionary history of nature, and then using them as a space and electronic structure blueprints for design of the artificial carbon-fixing catalyst.

The biological redox conversion of CO_2, N_2, O_2 and H_2 is an important process in our planet's biogeochemical cycles and has a fairly long history. A wide range of evidence suggests that both the existence of the biosphere today and the origin of the earliest life forms on Earth depends on its capacity to fix inorganic CO_2 into living

matter[16,17]. According to reports, seven carbon fixation pathways in nature have been discovered. The Calvin cycle[18], which combined with photosynthesis are the workhorses of large-scale CO_2 fixation in nature, was first recognized in 1948, followed by the reverse krebs cycle[19] (reverse TCA cycle) in 1966, the reductive acetyl-CoA pathway[20] (Wood–Ljungdahl pathway) in 1972, the 3-hydroxypropionate bicycle[21] (3-HP/malyl-CoA cycle) in 1993, the dicarboxylate/4-hydroxybutyrate cycle[22] in 2007 (Di-4HB cycle), the 3-hydroxypropionate-4-hydroxybutyrate cycle[23] in 2008 (3HP-4HB cycle), and the enoyl-CoA carboxylases/reductases[24] in 2016. Among the seven known CO_2 fixation pathways in nature, the acetyl-CoA (Wood–Ljungdahl pathway) pathway is one of the most ancient, and relies on metalloenzymes containing transition metal active centers for CO_2 activation[25]. This kind of ancient metalloenzyme is named Carbon monoxide dehydrogenase/acetyl-CoA synthases (CODHases/ACSs), it may be the earliest biological carbon-fixing enzyme evolved by natural thermophilic anaerobic microorganisms in the autotrophic theory of the origin of life[26-28], supporting the ability of early organisms to live in the CO_2-rich atmosphere that existed during the Archean Eon[29,30].

Herein, inspired by the crystal structure of CO dehydrogenase II[31] isolated from *Carboxyothermus hydrogenoformans* ($CODHII_{Ch}$) at 1.50 Å resolution, we designed a heterogeneous Fe_4S_4 single-cluster catalyst Ni100-Fe_4S_4 for the electrocatalytic reduction of CO_2. Compared with gaseous CO_2 and adsorbed CO_2 in $CODHII_{Ch}$ from crystallographic analysis measured in the past reported experiments[31,32], the adsorbed CO_2 on Ni100-Fe_4S_4 by first-principles calculation exhibits longer bond lengths and

smaller bond angles, which endows Ni100-Fe_4S_4 a better CO_2 activation. Furthermore, charge difference and density of states (DOS) analysis indicated that the electrons of Ni atoms and Fe_4S_4 iron-sulfur cluster on the Ni (100) surface aggregated to the heterojunction interface, forming a highly active electron-rich Fe-Ni 'electro-bridge' catalytic site. Encouragingly, this special biomimetic Fe-Ni 'electro-bridge' catalytic site can activate CO_2 molecules efficiently, stabilizing various intermediates in multistep elementary reactions to produce CH_4 in a low overpotential selectively. The electroreduction calculation results can completely consistent with the nickel-based catalytic materials reported in the current experiments[33-36]. This rational design of Ni100-Fe_4S_4 catalyst skillfully combines the biology advantages of natural enzymes with the concepts of modern catalytic science, opening an avenue for development of efficient artificial carbon fixation catalysts.

■ COMPUTATIONAL DETAILS

All spin-polarized DFT calculations for periodic material systems were performed with the Vienna Ab initio simulation package (VASP)[53,54] using the projector-augmented wave (PAW) method[55]. The exchange–correlation function was handled using the generalized gradient approximation (GGA) formulated by the Revised Perdew-Burke-Ernzerhof (RPBE)[56]. The van der Waals (vdW) interactions are described with the DFT-D3 method in Grimme's scheme[57,58]. The interaction between the atomic core and electrons was described by the projector augmented wave method. The plane-wave basis set energy cutoff was set to 500 eV. The Brillouin zone was sampled with a 2 × 3 × 1

grid centered at the gamma (Γ) point for geometry relaxation. The perfect Ni bulk was fully optimized using 16 × 16 × 16 k-point Gamma (Γ) centered Monkhorst-Pack mesh sampling. The Ni (100) facets were modeled using a four-layer 4 × 3 slab containing 96 atoms with 13.91 Å × 10.43 Å in x and y directions, respectively, and a 15 Å vacuum region, ensuring negligible lateral interaction of adsorbates. Fe_4S_4 cluster absorbs on the Ni (100) surface, with a 13.91 Å × 10.43 Å × 20.22 Å simulation boxes containing 107 atoms, the bottom two layers were kept frozen at the lattice position. All structural models with a dynamic magnetic moment were fully relaxed to optimize without any restriction until their total energies gradient were converged to < 1×10^{-5} eV, and the average residual forces were < 0.02 eV/Å. Moreover, the Gibbs free energy calculation is operated with computational hydrogen electrode (CHE) model[59], and the solvent effect is considered with the implicit solvent model implemented in VASPsol[60,61]. The position-specific charge values are obtained using Bader analysis.

■ RESULTS AND DISCUSSION

Designing catalysts by learning from nature. Nature provides a blueprint to efficiently activate CO_2 molecules and selectively generate useful fuels and value-added chemical feedstocks using metalloenzymes. To accelerate high-performance CO_2RR catalysts discovery, we propose a method for the rational design of catalysts assisted by 'nature blueprints'. In this study, a dehydrogenase separated from *Carboxyothermus hydrogenoformans* (a bacterium isolated from a Russian hotspring[37]) was used as a 'nature blueprint' to aid in the structural design of Ni100-Fe_4S_4 (Fig. 1). CO

dehydrogenases (CODHases) are the biological catalysts for the reversible oxidation of CO_2 to CO[31]:

$$CO_2(g) + 2H^+ + 2e^- \xleftrightarrow{CODHases} CO(g) + H_2O(l) \quad (1)$$

Figure 1a shows the crystal structure of CO dehydrogenase II, which contains a special asymmetric [Ni-4Fe-5S] cluster. In the detailed crystal structure experimental data[31,38], the structure of $CODHII_{Ch}$ with CO_2 reveals a triatomic ligand bridging Fe and Ni (Fig. 1b,1c). This Fe-Ni bimetallic factor often plays a synergistic role in the catalytic reaction[39,40], which is beneficial to the activation and catalytic conversion of CO_2. Based on this special asymmetric [Ni-4Fe-5S] cluster enzymatic active center, we designed a heterogeneous catalyst Ni100-Fe_4S_4 by Fe_4S_4 loading single-clusters on the Ni (100) surface. The calculation results show that the Fe-O bonds (2.04 Å) and Ni-C bonds (1.99 Å) formed after the Ni100-Fe_4S_4 catalyst adsorbs CO_2 are only 0.01 Å and 0.03 Å different from those experimentally measured in the $CODHII_{Ch}$ (Fe-O 2.05 Å, Ni-C 1.96 Å), respectively (Fig. 1c,1d). The similar adsorption bond length means that Ni100-Fe_4S_4 and $CODHII_{Ch}$ have the same CO_2 binding mode, indicating that the Ni100-Fe_4S_4 catalyst may have an enzyme-like catalytic activity.

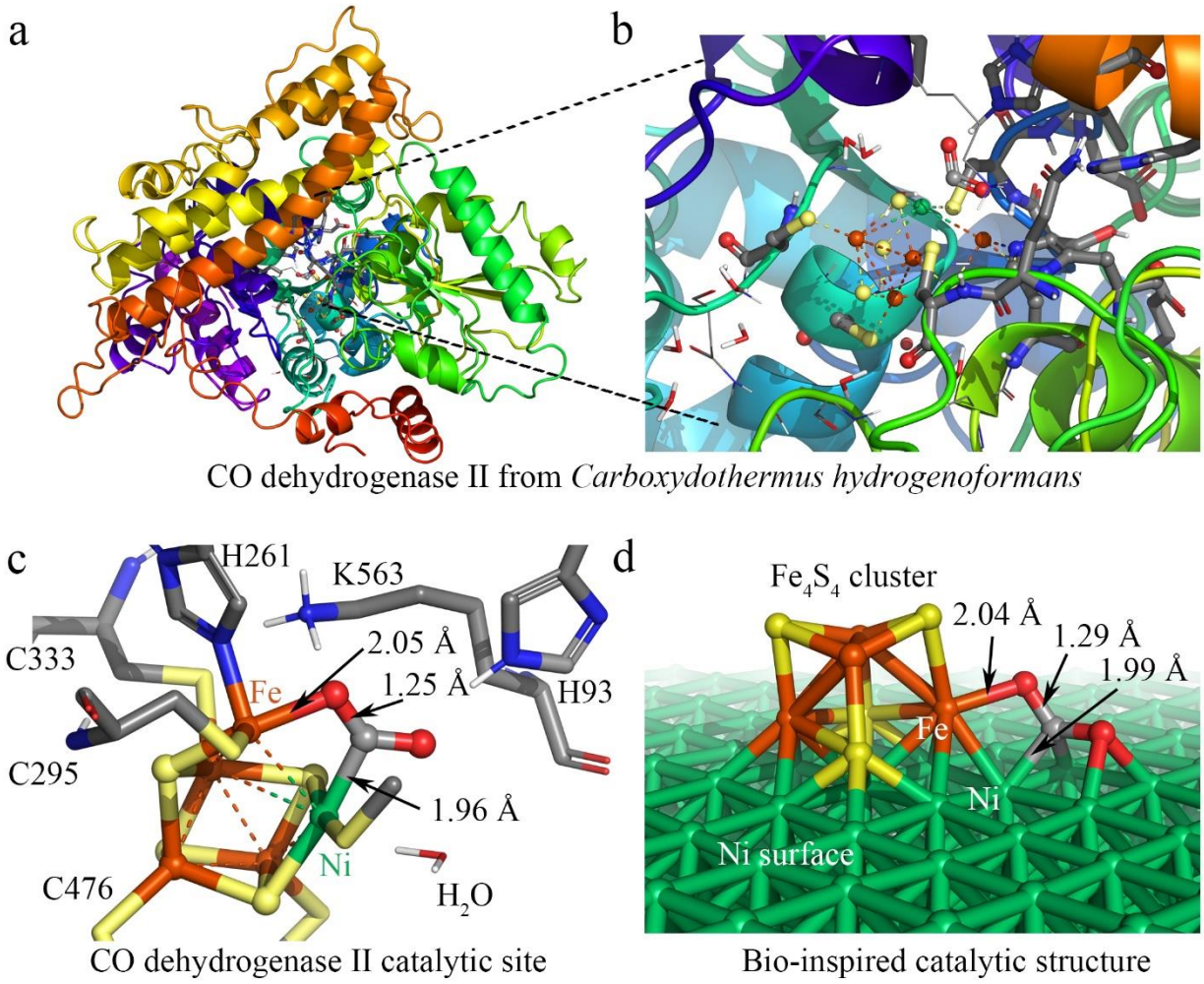

Figure 1. Design of Ni100-Fe_4S_4 catalyst inspired by CO dehydrogenase II. (a) The crystal structure of $CODHII_{Ch}$. (b) The catalytic center of $CODHII_{Ch}$. (c) The structure of $CODHII_{Ch}$ catalytic center combined with CO_2. (d) The structure of bio-inspired heterogeneous Ni100-Fe_4S_4 catalyst. (In atomic coloring, the white is H, the gray is C, the blue is N, the red is O, the yellow is S, the orange is Fe, and the green is Ni)

Activating CO_2 beyond nature. The electroreduction of carbon dioxide by the catalyst preferentially determined by the ability and degree of CO_2 activation. To activate CO_2 molecules, the active site basically needs to have the ability to adsorb CO_2. Since gaseous CO_2 molecules exhibit a linear shape and have stable triple-center π bonds

(Fig. 2), ordinary physical adsorption hardly changes their geometric and electronic structures. Therefore, the activation of CO_2 molecules requires stronger chemisorption, and most forms of chemisorption will change the bond length and bond angle of CO_2 molecules, resulting in the splitting of its three-center π bond. The geometric and electronic structures are subsequently changed, exhibiting a metastable activated CO_2 molecule.

As shown in Fig. 2, the crystal structure obtained by rotating anode x-ray diffraction[31] shows that the CO_2 molecules adsorbed on the catalytic active site of $CODHII_{Ch}$ are no longer linear in gaseous CO_2. Its ∠O-C-O angle is 133°, and the C-O bond length is elongated from 1.16 Å to 1.25 Å compared with gaseous CO_2 molecules. Interestingly, in the structure of Ni100-Fe_4S_4 adsorbing CO_2, its ∠O-C-O angle is smaller than that in $CODHII_{Ch}$, only 119°, and the C-O bond is also longer, reaching 1.29 Å. Smaller ∠O-C-O angle and longer C-O bonds indicate that the Ni100-Fe_4S_4 designed inspired by the active center structure of $CODHII_{Ch}$ exhibits stronger CO_2 activation ability.

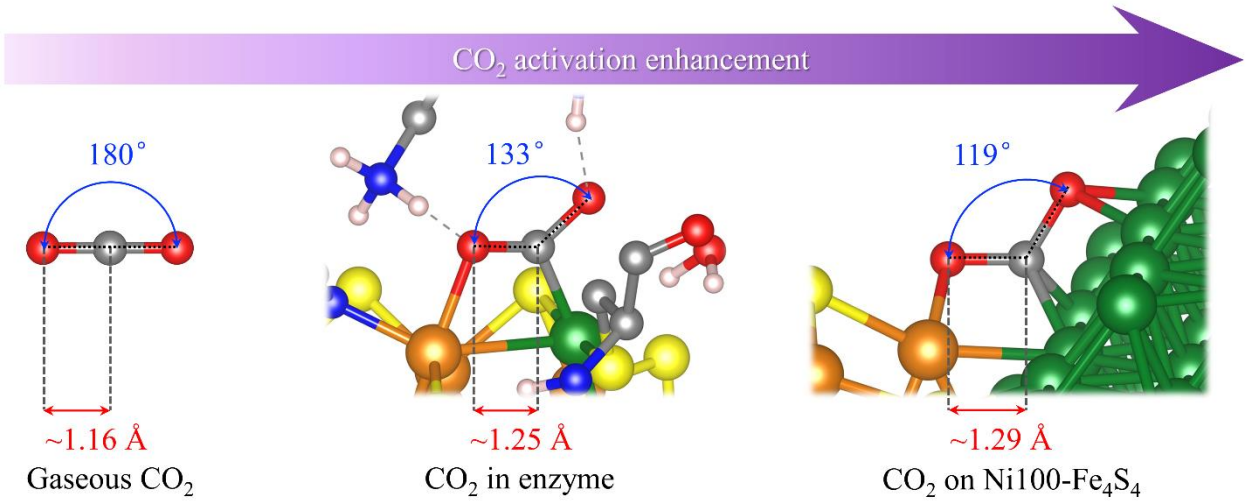

Figure 2. Schematic diagram of geometric structure of CO_2 in different adsorption states

and CO_2 activation enhancement.

Fe-Ni 'electro-bridge' enhanced CO_2 activation. Bio-inspired strategies to control the performance of CO_2 activation focuses on the geometric and electronic structure of the active site. We applied this methodology to the design of Ni100-Fe_4S_4. Fig. 3a shows top view, front view and side view of Ni100-Fe_4S_4 catalyst structure, which was by loading Fe_4S_4 iron-sulfur clusters onto the Ni (100) surface. The geometric structure is the global energy minimum obtained by spin-polarized first-principles calculations. This iron-sulfur clusters, which are commonly used in biology to transfer electrons, are stabilized on Ni (100) surface to form a special Ni100-Fe_4S_4 cluster-interface heterojunction structure.

To unveil the origin of the structural activity of the Ni100-Fe_4S_4 heterojunction, we further calculated the projected density of states (PDOS) onto the *p* and *d* states of Ni100-Fe_4S_4 (Fig. 3b). In the PDOS of Ni100-Fe_4S_4, the peak near the Fermi level is mainly composed of Fe and Ni, implying that Fe-Ni is a highly active site. The Fe-Ni site in Ni100-Fe_4S_4 mimic the Fe-Ni catalytic sites in $CODHII_{Ch}$, which are crucial for CO_2 activation and reaction selectivity. Owing to the interaction of the heterojunction interface between Ni (100) and Fe_4S_4, the surface Ni atoms and Fe_4S_4 iron-sulfur clusters could transfer charge to Fe-Ni site and an optimized polarization field is generated on its surface.

Furthermore, charge difference analysis results show that a large number of electrons are transferred from Fe_4S_4 iron-sulfur cluster and Ni (100) surface to Fe-Ni

site, forming a highly active electron-rich Fe-Ni 'electro-bridge' catalytic site on the heterojunction interface (Fig. 3c-3f). Therefore, the Fe-Ni site can inject enough electrons into the CO_2 2π* antibonding orbitals, disrupting the strong *sp*-hybridization symmetry of the carbon atom.

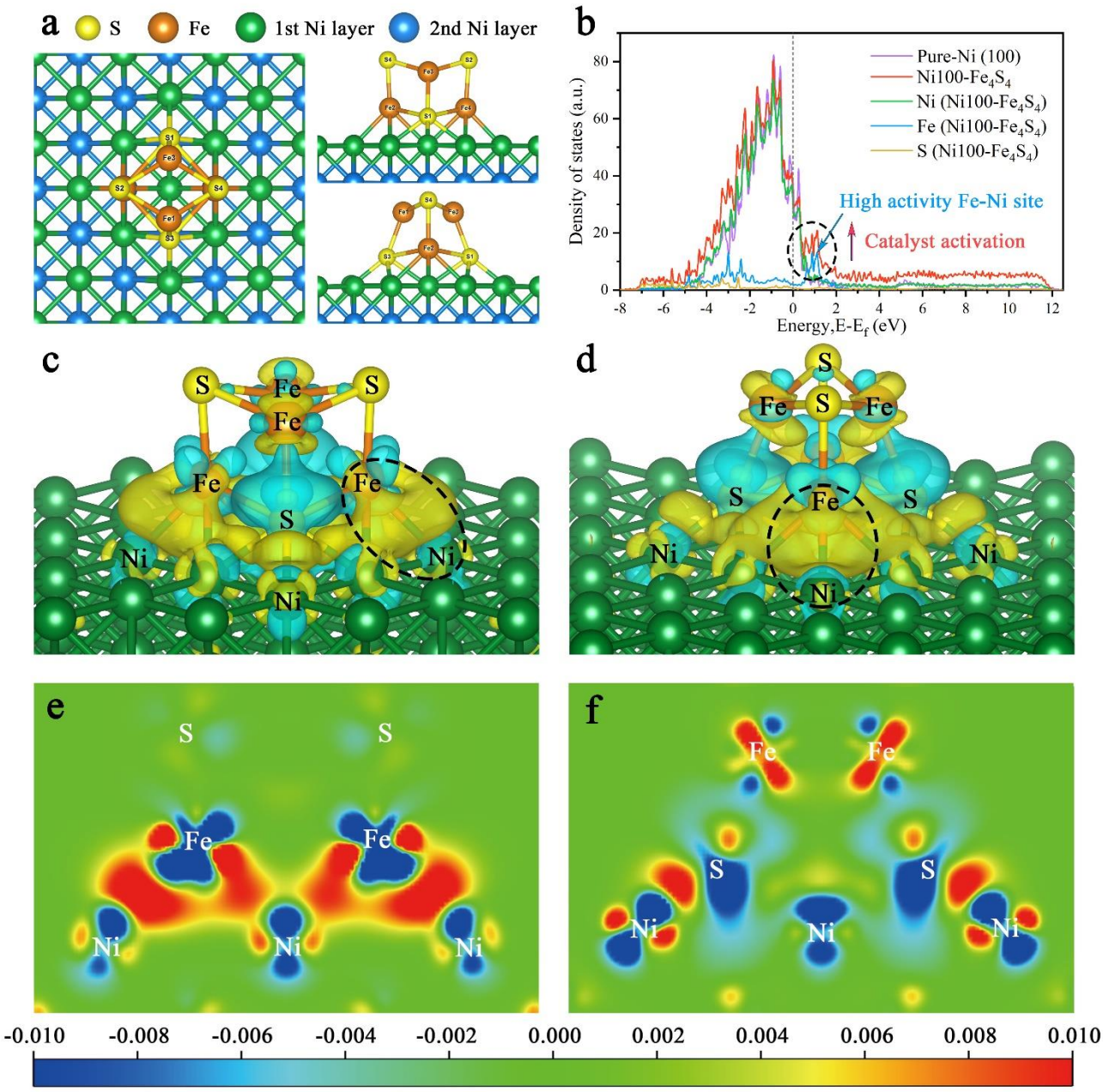

Figure 3. The geometric and electronic structure of the Ni100-Fe_4S_4. (a) The geometric structure of Ni100-Fe_4S_4. (b) The projected density of states (PDOS) onto the *p* and *d*

states of Ni100-Fe_4S_4. (c, d) The charge difference analysis of Ni100-Fe_4S_4 catalyst. (Light blue and yellow stands for outflow and inflow of electrons, respectively. The black dotted circle represents Fe-Ni 'electro-bridge'.) (e, f) The tangent plane of charge difference in Ni100-Fe_4S_4 catalyst. (Blue stands for outflow and red for inflow of electrons.)

The mechanism of CO_2 adsorption and activation. Based on above designed structure by bio-inspired strategies, the adsorption models for theoretical calculations can be constructed to have insights into to the CO_2 adsorption step on Ni100-Fe_4S_4 from an atomic/electronic-level standpoint. Specifically, the thermodynamic energy conversion, *d*-band center, work function and electron-density isosurfaces were performed to theoretically and systematically reveal the mechanism of the CO_2 adsorption step on Ni100-Fe_4S_4. To shed light on the characteristics and performance of Ni100-Fe_4S_4 adsorption of CO_2, we first analyzed the adsorption energy (The equation is Supplementary S1). As depicted in Fig. 4a, Ni100-Fe_4S_4 shows a much significant thermodynamic energy conversion of CO_2 adsorption step (-0.56 eV) than pure Ni (100) (-0.44 eV). The pure Ni (100) has been widely proved to be a good CO_2 adsorbent both theoretically and experimentally[33,41-43]. This means Ni100-Fe_4S_4 tends to well adsorb CO_2 in theory, which is well in line with the *d*-band center (Fig. 4d, The equation is Supplementary S2). The favorable adsorption of CO_2 on Ni100-Fe_4S_4 will accelerate its CO_2RR processes and promote its CO_2RR activity.

To investigate the electronic structure and surface adsorption behavior on Ni100-

Fe_4S_4, we calculated the electron-density isosurface (Fig. 4b,4c) and the electronic work function (Fig. 4e,4f) for Ni100-Fe_4S_4 and Ni100-Fe_4S_4-*CO_2, respectively. The work function is an essential physical property of metallic materials[44], which has been widely used in the design and evaluation of various photo/electrocatalysts[45,46], can be obtained by calculating the difference between the electrostatic potential at the vacuum level E_{vac} and the electrostatic potential at the Fermi level E_F using Supplementary Equations S4 and S5. The detailed electrostatic potential and work function calculation formula are given in Supplementary S3, S4. As shown in Fig. 4b, 4c, the work function of Ni100-Fe_4S_4 increases from 4.83 eV to 5.08 eV after CO_2 adsorption, which means that the electrons on the surface of Ni100-Fe_4S_4 flow to the CO_2 molecule increasing the work function of the system. According to past reports, the surface energy of the system is inversely proportional to the work function[47]. Therefore, the adsorption step of CO_2 on Ni100-Fe_4S_4 simultaneously reduces the surface energy of the system and increases the stability of the material surface. Meanwhile, the electron-density isosurface demonstrates that the Fe-Ni sites with lower electrostatic potential (Fig. 4e, black dotted circle area) on the Ni100-Fe_4S_4 surface are favorable for the nucleophilic attack on the electrophilic carbonyl carbon of CO_2 molecules. In addition, the electrostatic potentials around the isosurface of the O atom of CO_2 are at a low level (Fig. 4f, black dotted circle area), indicating a selective hydrogenation site.

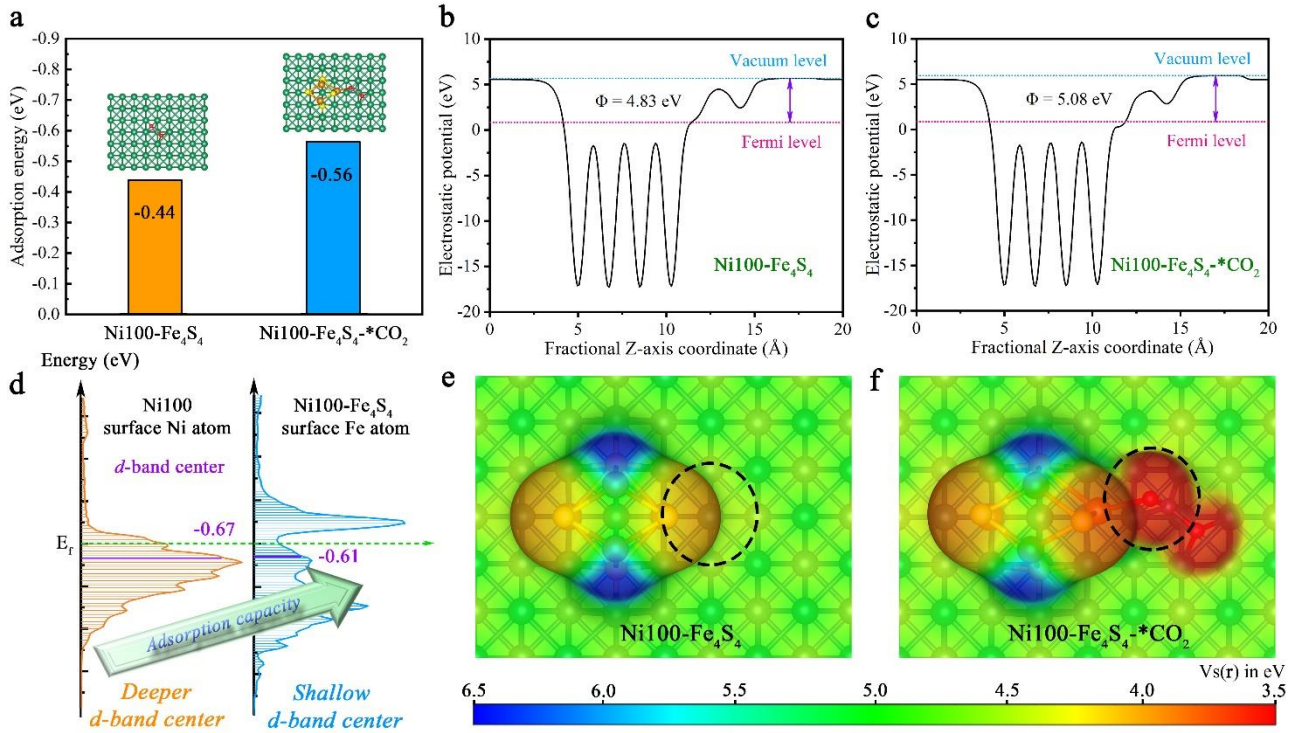

Figure 4. The adsorption energy, *d*-band center, surface electrostatic potential and work function analysis of CO_2 adsorption. (a) Comparison of adsorption energy between Ni (100) and Ni100-Fe_4S_4. (b) The work function of Ni100-Fe_4S_4. (c) The work function of Ni100-Fe_4S_4-*CO_2. (d) Comparison of *d*-band center between Ni atom on Ni (100) and Fe atom on Ni100-Fe_4S_4. (e) Electron-density isosurface of Ni100-Fe_4S_4. (f) Electron-density isosurface of Ni100-Fe_4S_4*-CO_2. The color bar stands for the scale of electrostatic potential and the isosurfaces are plotted at 0.002 e·bohr^{-3} level.

Also, we calculated the charge distribution of Ni100-Fe_4S_4-*CO_2. As presented in Fig. 5a, we can clearly observe that the electron inflow into two O atoms of the adsorbed CO_2 in Ni100-Fe_4S_4-*CO_2 by the charge density difference. Further Bader charge analysis showed that electrons flowed mainly from Fe atoms to CO_2 molecules attributed to the large spin polarization on Fe (Fig. 5b), which is consistent with the

electron-density isosurface and work function analysis. Remarkably, in this charge transfer mode, the C atom of the CO_2 molecule has a highly positive charge (+2.21 *e*), and the oxygen atom has a highly negative charge (-1.76 *e* and -1.62 *e*), which means that the most negative charge oxygen atomic site (-1.76 *e*) is more favorable for the subsequent electrocatalytic step to combine with H^+. This selectivity of hydrogenation site is consistent with subsequent Gibbs free energy calculations (Fig. 6, Supplementary Table S1, Table S4).

To elucidate the bonding nature of the CO_2 molecules and Ni100-Fe_4S_4 involved in the associative mechanism, we further calculated the densities of states (DOS) of Ni100-Fe_4S_4-*CO_2 and Fe-Ni_4 site (five atoms in Ni100-Fe_4S_4 directly affected by CO_2 molecule) for comparison (Fig. 5c). By comparing the DOS and molecular orbitals of the gaseous linear CO_2 molecule and the activated bent CO_2 molecule, we found that the π orbital, *n* orbital and π* orbital of the CO_2 molecule were split after activation. The π* orbital splits into two empty orbitals with unequal energy levels in the activated CO_2 molecule, which are well matched with the Fe-Ni_4 polarized β-spin *d* orbitals near the Fermi level, forming a partial occupation *d*-π* hybrid orbitals. Although the energy levels of Fe-Ni_4's majority α-spin *d* orbitals are about 2.0 eV lower than the π* orbitals of activated CO_2, the results show that the interaction between the α orbitals and the π* orbitals is obvious. This α-orbital interaction is due to the fact that there are still minority α orbitals present near the Fermi level, matching the π* orbitals of CO_2 molecule. This CO_2 activation mechanism reveals that the electrons from *d* orbitals of Ni100-Fe_4S_4 partially transfer to the empty π* orbitals of adsorbed CO_2, which is consistent with the

charge density difference analysis (Fig. 5a) and the DOS analysis (Fig. 5c).

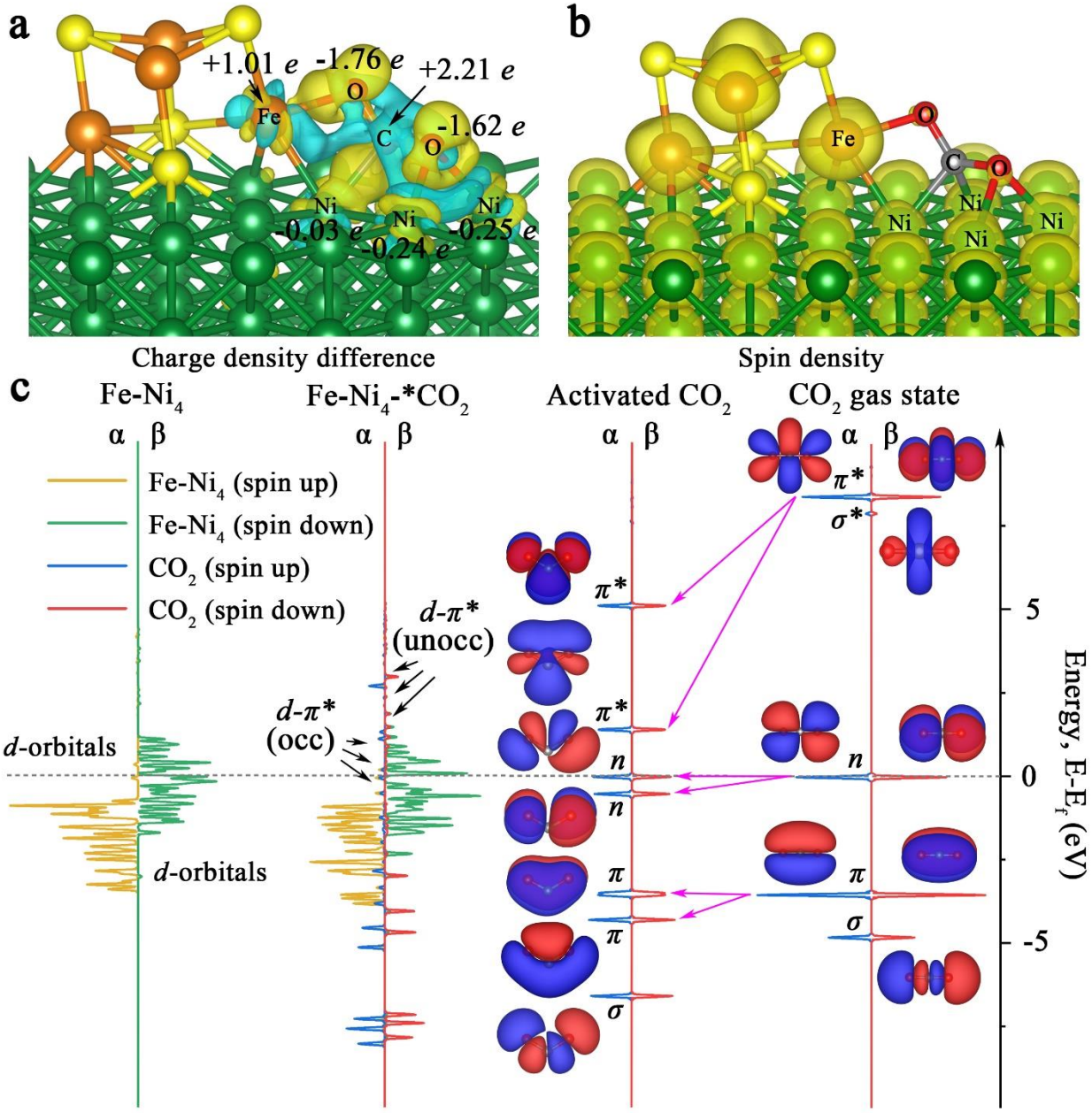

Figure 5. Associative and activation mechanism analysis. (a) Charge density difference of CO_2 adsorption on Ni100-Fe_4S_4. (Light blue stands for outflow and yellow for inflow of electrons) (b) Spin density of Ni100-Fe_4S_4. (Yellow stands for spin electrons) (c) Projected electronic densities of states (PDOS) of $FeNi_4$, CO_2 and their interactive

configuration $FeNi_4$-*CO_2.

Reaction mechanism of CO_2 electroreduction to CH_4. In order to further evaluate the activity and selectivity of Ni100-Fe_4S_4 to convert CO_2* to hydrocarbon species, we studied the free energy changes (ΔG) of the entire CO_2 reduction catalytic cycles. We first considered the adsorption pattern of CO_2 molecules on the Ni100-Fe_4S_4 surface (Supplementary Fig. S1, Table S4), DFT calculations showed that CO_2 molecules tended to be in the C-O site adsorption pattern (Supplementary Fig. S1c) rather than the O-O site (Supplementary Fig. S1a) adsorption pattern. This adsorption pattern is consistent with previously reported Ni-based materials[41,42]. Then, the free energy calculation results (Fig. 6a) confirmed that the first hydrogenation step of CO_2RR is preferentially on O to form COOH* rather than C (OCHO*) due to the low level of electrostatic potentials around the isosurface of the O atom of CO_2 (Fig. 4f, black dotted circle area, Supplementary Table S4). In the entire hydrogenation steps and reduction mechanism of CO_2, CO_2RR on Ni100-Fe_4S_4 following the circulation pathway of * → CO_2* → COOH* → CO* → CHO* → CH_2O* → CH_3O* → O* → OH* → H_2O* → *, with the final product of CH_4 (Fig. 6b). With this Ni100-Fe_4S_4 catalyst, the potential determining step (PDS) is CO* → CHO*, and the entire catalytic cycle with a limiting potential of only 0.13 eV, which is much lower than those most reported CO_2RR catalysts in recent years (Supplementary Table S2). Therefore, Ni100-Fe_4S_4 is potentially an efficient CO_2RR catalyst producing CH_4 in a low overpotential selectively.

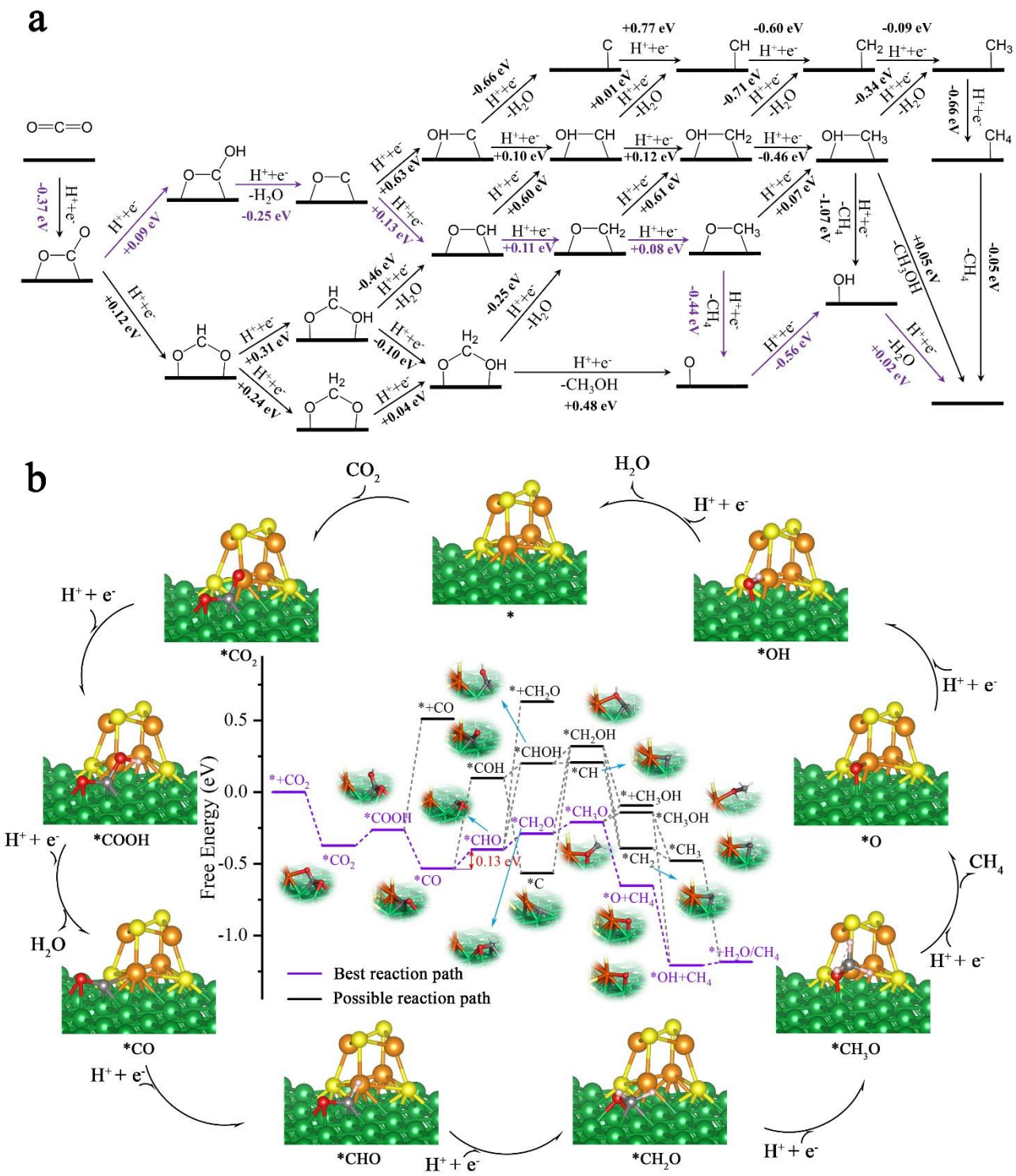

Figure 6. The CO_2RR paths on Ni100-Fe_4S_4. (a) The free energy changes (ΔG) of the entire possible CO_2RR paths, the energy optimal route is marked in purple. (b) The schematic diagram of the Reaction mechanism of CO_2 electroreduction to CH_4 in entire CO_2 reduction catalytic cycles.

Selectivity for CO_2 electroreduction. In order to study the stability of cluster and the selectivity of catalyst, we considered side reactions involving hydrogen evolution reaction (HER) and H_2S evolution reaction (H_2SER). HER is an important competing side reaction, which can constantly consume proton–electron pairs from the electrolyte solution, restraining the faradaic efficiency of CO_2RR significantly[7,48,49]. To identify possible HER side-reaction sites, we first calculated Gibbs free energy changes (ΔG) of HER ($* + H^+ + e^- \rightarrow H^*$) on Fe-Ni site, Fe site, Ni site and S site (Fig. 7a, Supplementary Table S4). According to the Brønsted–Evans–Polanyi relation[50,51], the result shows that the Fe-Ni site with a lower ΔG= -0.15 eV, which are kinetically more favored due to the smaller reaction barriers. Besides, the calculated results show that hydrogenation is preferentially on O to form COOH* rather than C (OCHO*) both thermodynamically and kinetically (Supplementary Table S4, Fig. 4). So, we compare HER with the first hydrogenation step of CO_2RR at ($* + CO_2(g) + H^+ + e^- \rightarrow COOH^*$). The heatmap diagram of the Gibbs free energy changes (Fig. 7c) indicate that Ni100-Fe_4S_4 have a higher selectivity toward CO_2RR.

H_2S evolution reaction is a possible dissociation event on Fe_4S_4 clusters[52]. To test the stability of Ni100-Fe_4S_4, we calculated and plotted the free energy of H_2SER in Fig. 7b and Supplementary Table S4. The calculated thermodynamic energy barrier is quite large ΔG= +1.94 eV, which suggests that the H_2SER on Ni100-Fe_4S_4 is both thermodynamically and kinetically difficult. Therefore, the analysis results of side reactions demonstrate the Ni100-Fe_4S_4 catalyst is promising as a cathode material for

CO_2RR with high selectivity and Faradaic efficiency.

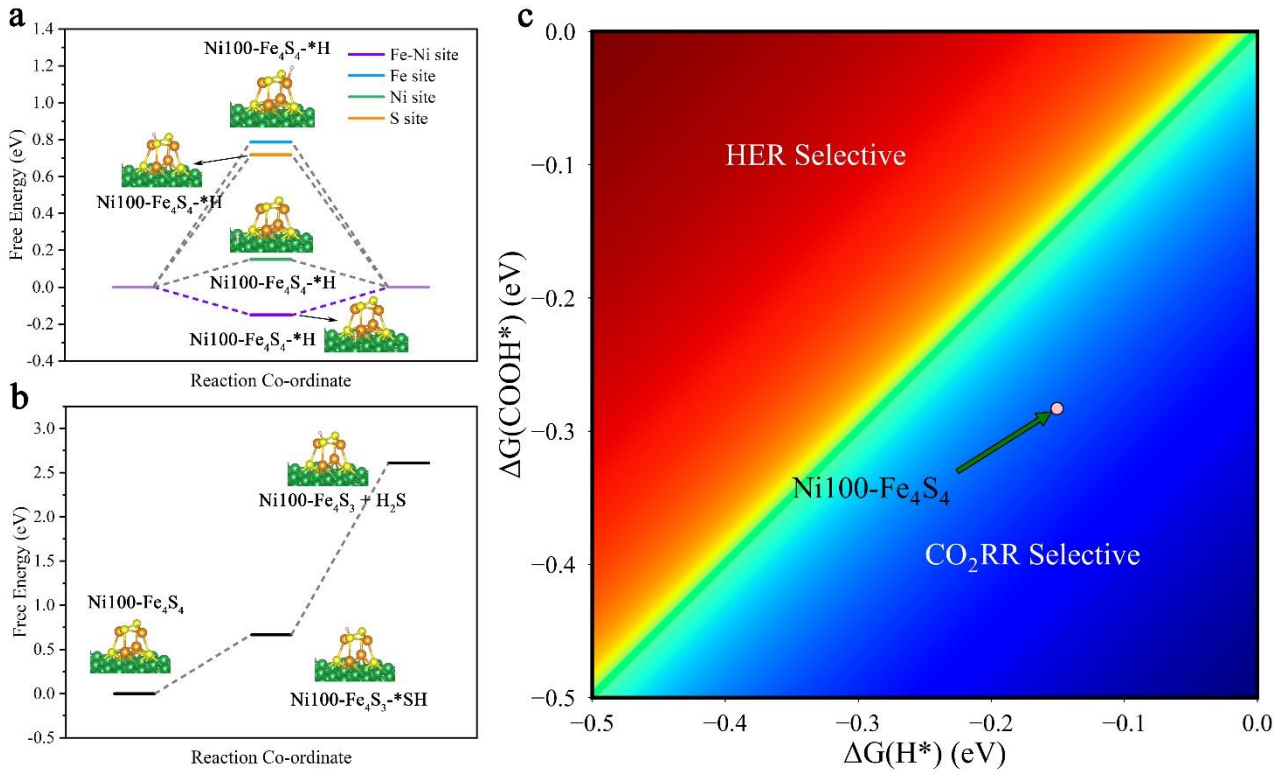

Figure 7. Selectivity between CO_2RR, HER and H_2SER. (a) Free energy diagrams of possible HER mechanisms on Fe-Ni site, Fe site, Ni site and S site. (b) Free energy diagrams of possible H_2SER mechanisms on cluster. (c) Selectivity for CO_2RR vs HER, the light pink data points represent Ni100-Fe_4S_4 catalyst, the blue region represent higher selectivity to CO_2RR, while the red region to HER.

■ CONCLUSION

In conclusion, we have developed a 'nature blueprints' aided material design method. Taking Ni100-Fe_4S_4 as an example, we designed this heterogeneous Fe_4S_4 single-cluster catalyst by imitating the spatial structure of the Fe, Ni active center in CO dehydrogenase II from *Carboxyothermus hydrogenoformans*. We found that Ni100-

Fe_4S_4 exhibits stronger CO_2 activation ability than the natural CO dehydrogenase by analyzing the changes of CO_2 adsorption state, geometric structure and electronic structure. This excellent CO_2 activation ability of Ni100-Fe_4S_4 is mainly attributed to the Fe-Ni site designed by the bio-inspired strategy, forming a Fe-Ni 'electro-bridge' enhanced CO_2 activation. The detail electronic structure analysis shows that the electrons from Fe-Ni site's *d* orbitals partially transfer to the empty π* orbitals of CO_2, leading to partial occupation of the formed *d*-π* orbitals. Moreover, the free energy changes (ΔG) of the entire CO_2 reduction catalytic cycles were calculated. The detail study on reaction mechanism of CO_2 electroreduction shows that CO_2RR on Ni100-Fe_4S_4 following the circulation pathway of * → CO_2* → COOH* → CO* → CHO* → CH_2O* → CH_3O* → O* → OH* → H_2O* → *, with the final product of CH_4. To be more rigorous, the side reactions involving hydrogen evolution reaction (HER) and H_2S evolution reaction (H_2SER) was also calculated and proved to be thermodynamically unfavorable. These promising results show the feasibility of using Ni100-Fe_4S_4 catalyst as cathodes for CO_2RR with a high selectivity and faradaic efficiency. Therefore, the bio-inspired strategies as a transformative approach which can be directly applied to heterogeneous catalysts. Clever use these 'nature blueprints' in modern catalyst design will lead our catalysts beyond its current limitations exploring the final frontier of catalysis.

■ ASSOCIATED CONTENT

■ Supporting Information

Supplementary material for this article is available at Supplementary Information.pdf

■ AUTHOR INFORMATION

Corresponding Authors

Lan Ma - *Institute of Biopharmaceutical and Health Engineering, Tsinghua Shenzhen International Graduate School, Tsinghua University, Shenzhen 518055, China; Institute of Biomedical Health Technology and Engineering, Shenzhen Bay Laboratory, Shenzhen 518055, China;* orcid.org/0000-0002-6610-5871; Email: malan@sz.tsinghua.edu.cn

Authors

Hengyue Xu - *Institute of Biopharmaceutical and Health Engineering, Tsinghua Shenzhen International Graduate School, Tsinghua University, Shenzhen 518055, China;* orcid.org/0000-0003-4438-9647; Email: xuhy21@mails.tsinghua.edu.cn

Author contributions

H.X. conceived the idea of the designing of bio-inspired Ni100-Fe_4S_4 catalyst. H.X. performed all calculations and analyzed the data. H.X. wrote the initial manuscript and L.M. revised the initial manuscript to the final version. L.M. provided funding and platform support for research projects. L.M. gave many valuable suggestions and guidance on the subject and reviewed the manuscript in details.

Notes

The authors declare no competing interests.

■ ACKNOWLEDGMENTS

This research was funded by the Institute of Biomedical Health Technology and Engineering, Shenzhen Bay Laboratory. We are grateful to Shenzhen Bay Laboratory Supercomputing Center for providing high performance computing platform.

■ REFERENCES

(1) Cox, P. M.; Betts, R. A.; Jones, C. D.; Spall, S. A.; Totterdell, I. J. Acceleration of global warming due to carbon-cycle feedbacks in a coupled climate model. *Nature* **2000,** *408* (6809), 184.

(2) Humphrey, V.; Zscheischler, J.; Ciais, P.; Gudmundsson, L.; Sitch, S.; Seneviratne, S. I. Sensitivity of atmospheric CO2 growth rate to observed changes in terrestrial water storage. *Nature* **2018,** *560* (7720), 628.

(3) Montañez, I. P.; Tabor, N. J.; Niemeier, D.; DiMichele, W. A.; Frank, T. D.; Fielding, C. R.; Isbell, J. L.; Birgenheier, L. P.; Rygel, M. C. CO2-forced climate and vegetation instability during Late Paleozoic deglaciation. *Science* **2007,** *315* (5808), 87.

(4) Thomas, C. D.; Cameron, A.; Green, R. E.; Bakkenes, M.; Beaumont, L. J.; Collingham, Y. C.; Erasmus, B. F.; De Siqueira, M. F.; Grainger, A.; Hannah, L. Extinction risk from climate change. *Nature* **2004,** *427* (6970), 145.

(5) Seh, Z. W.; Kibsgaard, J.; Dickens, C. F.; Chorkendorff, I.; Norskov, J. K.; Jaramillo, T. F. Combining theory and experiment in electrocatalysis: Insights into materials design. *Science* **2017,** *355* (6321), 1.

(6) Birdja, Y. Y.; Pérez-Gallent, E.; Figueiredo, M. C.; Göttle, A. J.; Calle-Vallejo, F.; Koper, M. T. M. Advances and challenges in understanding the electrocatalytic conversion of carbon dioxide to fuels. *Nat. Energy* **2019,** *4* (9), 732.

(7) Zhong, M.; Tran, K.; Min, Y.; Wang, C.; Wang, Z.; Dinh, C.-T.; De Luna, P.; Yu, Z.; Rasouli, A. S.; Brodersen, P.et al. Accelerated discovery of CO2 electrocatalysts using active machine learning. *Nature* **2020,** *581* (7807), 178.

(8) Tran, K.; Ulissi, Z. W. Active learning across intermetallics to guide discovery of electrocatalysts for CO2 reduction and H2 evolution. *Nat. Catal.* **2018,** *1* (9), 696.

(9) Sun, Y.; Liao, H.; Wang, J.; Chen, B.; Sun, S.; Ong, S. J. H.; Xi, S.; Diao, C.; Du, Y.; Wang, J.-O.et al. Covalency competition dominates the water oxidation structure–activity relationship on spinel oxides. *Nat. Catal.* **2020,** *3* (7), 554.

(10) Shafaat, H. S.; Yang, J. Y. Uniting biological and chemical strategies for selective CO2 reduction. *Nat. Catal.* **2021,** *4* (11), 928.

(11) Wang, H.-B.; Wang, J.-Q.; Zhang, R.; Cheng, C.-Q.; Qiu, K.-W.; Yang, Y.-j.; Mao, J.; Liu, H.; Du, M.; Dong, C.-K.et al. Bionic Design of a Mo(IV)-Doped FeS2 Catalyst for Electroreduction of

Dinitrogen to Ammonia. *ACS Catal.* **2020,** *10* (9), 4914.
(12) Zhang, H.; Huang, L.; Chen, J.; Liu, L.; Zhu, X.; Wu, W.; Dong, S. Bionic design of cytochrome c oxidase-like single-atom nanozymes for oxygen reduction reaction in enzymatic biofuel cells. *Nano Energy* **2021,** *83*.
(13) Cesana, P. T.; Li, B. X.; Shepard, S. G.; Ting, S. I.; Hart, S. M.; Olson, C. M.; Martinez Alvarado, J. I.; Son, M.; Steiman, T. J.; Castellano, F. N.et al. A biohybrid strategy for enabling photoredox catalysis with low-energy light. *Chem* **2022,** *8* (1), 174.
(14) Ren, C.; Yang, P.; Sun, J.; Bi, E. Y.; Gao, J.; Palmer, J.; Zhu, M.; Wu, Y.; Liu, J. A Bioinspired Molybdenum Catalyst for Aqueous Perchlorate Reduction. *J. Am. Chem. Soc.* **2021,** *143* (21), 7891.
(15) Weliwatte, N. S.; Minteer, S. D. Photo-bioelectrocatalytic CO2 reduction for a circular energy landscape. *Joule* **2021,** *5* (10), 2564.
(16) Braakman, R.; Smith, E. The Emergence and Early Evolution of Biological Carbon-Fixation. *PLoS Comput. Biol.* **2012,** *8* (4), e1002455.
(17) Berg, I. A.; Kockelkorn, D.; Ramos-Vera, W. H.; Say, R. F.; Zarzycki, J.; Hugler, M.; Alber, B. E.; Fuchs, G. Autotrophic carbon fixation in archaea. *Nat. Rev. Microbiol.* **2010,** *8* (6), 447.
(18) Calvin, M.; Benson, A. A. The Path of Carbon in Photosynthesis. *Science* **1948,** *107* (2784), 476.
(19) Evans, M.; Buchanan, B. B.; Arnon, D. I. A new ferredoxin-dependent carbon reduction cycle in a photosynthetic bacterium. *Proc. Natl. Acad. Sci. U.S.A.* **1966,** *55* (4), 928.
(20) Schulman, M.; Parker, D.; Ljungdahl, L. G.; Wood, H. G. Total synthesis of acetate from CO2 V. Determination by mass analysis of the different types of acetate formed from 13CO2 by heterotrophic bacteria. *J. Bacteriol.* **1972,** *109* (2), 633.
(21) Strauss, G.; Fuchs, G. Enzymes of a novel autotrophic CO2 fixation pathway in the phototrophic bacterium Chloroflexus aurantiacus, the 3-hydroxypropionate cycle. *Eur. J. Biochem.* **1993,** *215* (3), 633.
(22) Berg, I. A.; Kockelkorn, D.; Buckel, W.; Fuchs, G. A 3-hydroxypropionate/4-hydroxybutyrate autotrophic carbon dioxide assimilation pathway in Archaea. *Science* **2007,** *318* (5857), 1782.
(23) Huber, H.; Gallenberger, M.; Jahn, U.; Eylert, E.; Berg, I. A.; Kockelkorn, D.; Eisenreich, W.; Fuchs, G. A dicarboxylate/4-hydroxybutyrate autotrophic carbon assimilation cycle in the hyperthermophilic Archaeum Ignicoccus hospitalis. *Proc. Natl. Acad. Sci. U.S.A.* **2008,** *105* (22), 7851.
(24) Schwander, T.; Borzyskowski, L. S. v.; Burgener, S.; Cortina, N. S.; Erb, T. J. A synthetic pathway for the fixation of carbon dioxide in vitro. *Science* **2016,** *354* (6314), 900.
(25) Varma, S. J.; Muchowska, K. B.; Chatelain, P.; Moran, J. Native iron reduces CO2 to intermediates and end-products of the acetyl-CoA pathway. *Nat. Ecol. Evol.* **2018,** *2* (6), 1019.
(26) Can, M.; Armstrong, F. A.; Ragsdale, S. W. Structure, Function, and Mechanism of the Nickel Metalloenzymes, CO Dehydrogenase, and Acetyl-CoA Synthase. *Chem. Rev.* **2014,** *114* (8), 4149.
(27) Drennan, C. L.; Doukov, T. I.; Ragsdale, S. W. The metalloclusters of carbon monoxide dehydrogenase/acetyl-CoA synthase: a story in pictures. *J. Biol. Inorg. Chem.* **2004,** *9* (5), 511.
(28) Adam, P. S.; Borrel, G.; Gribaldo, S. Evolutionary history of carbon monoxide dehydrogenase/acetyl-CoA synthase, one of the oldest enzymatic complexes. *Proc. Natl. Acad. Sci. U.S.A.* **2018,** *115* (6), E1166.
(29) Catling, D. C.; Zahnle, K. J. The archean atmosphere. *Sci. Adv.* **2020,** *6* (9), eaax1420.
(30) Glasby, G. P. Earliest life in the Archean: rapid dispersal of CO2-utilizing bacteria from submarine hydrothermal vents. *Episodes* **1998,** *21* (4), 252.
(31) Jeoung, J.-H.; Dobbek, H. Carbon dioxide activation at the Ni, Fe-cluster of anaerobic carbon

monoxide dehydrogenase. *Science* **2007,** *318* (5855), 1461.
(32) Ogren, P. J. Using the asymmetric stretch band of atmospheric CO2 to obtain the C= O bond length. *J. Chem. Educ.* **2002,** *79* (1), 117.
(33) Gac, W.; Zawadzki, W.; Rotko, M.; Greluk, M.; Słowik, G.; Kolb, G. Effects of support composition on the performance of nickel catalysts in CO2 methanation reaction. *Catal. Today* **2020,** *357*, 468.
(34) Serrer, M.-A.; Gaur, A.; Jelic, J.; Weber, S.; Fritsch, C.; Clark, A. H.; Saraçi, E.; Studt, F.; Grunwaldt, J.-D. Structural dynamics in Ni–Fe catalysts during CO₂ methanation – role of iron oxide clusters. *Catal. Sci. Technol.* **2020,** *10* (22), 7542.
(35) Le, T. A.; Kim, M. S.; Lee, S. H.; Kim, T. W.; Park, E. D. CO and CO 2 methanation over supported Ni catalysts. *Catal. Today* **2017,** *293-294*, 89.
(36) Gao, Y.; Dou, L.; Zhang, S.; Zong, L.; Pan, J.; Hu, X.; Sun, H.; Ostrikov, K. K.; Shao, T. Coupling bimetallic Ni-Fe catalysts and nanosecond pulsed plasma for synergistic low-temperature CO2 methanation. *Chemical Engineering Journal* **2021,** *420*, 127693.
(37) Wu, M.; Ren, Q.; Durkin, A. S.; Daugherty, S. C.; Brinkac, L. M.; Dodson, R. J.; Madupu, R.; Sullivan, S. A.; Kolonay, J. F.; Nelson, W. C.et al. Life in Hot Carbon Monoxide: The Complete Genome Sequence of Carboxydothermus hydrogenoformans Z-2901. *PLoS Genet.* **2005,** *1* (5), e65.
(38) Dobbek, H.; Svetlitchnyi, V.; Gremer, L.; Huber, R.; Meyer, O. Crystal Structure of a Carbon Monoxide Dehydrogenase Reveals a [Ni-4Fe-5S] Cluster. *Science* **2001,** *293* (5533), 1281.
(39) Wang, Y.; Cao, L.; Libretto, N. J.; Li, X.; Li, C.; Wan, Y.; He, C.; Lee, J.; Gregg, J.; Zong, H.et al. Ensemble Effect in Bimetallic Electrocatalysts for CO2 Reduction. *J. Am. Chem. Soc.* **2019,** *141* (42), 16635.
(40) Li, J.; Huang, H.; Xue, W.; Sun, K.; Song, X.; Wu, C.; Nie, L.; Li, Y.; Liu, C.; Pan, Y.et al. Self-adaptive dual-metal-site pairs in metal-organic frameworks for selective CO2 photoreduction to CH4. *Nat. Catal.* **2021,** *4* (8), 719.
(41) Cai, J.; Han, Y.; Chen, S.; Crumlin, E. J.; Yang, B.; Li, Y.; Liu, Z. CO2 Activation on Ni(111) and Ni(100) Surfaces in the Presence of H2O: An Ambient-Pressure X-ray Photoelectron Spectroscopy Study. *J. Phys. Chem. C* **2019,** *123* (19), 12176.
(42) Farjamnia, A.; Jackson, B. The dissociative chemisorption of CO2 on Ni(100): A quantum dynamics study. *J. Chem. Phys.* **2017,** *146* (7), 074704.
(43) Zhou, X.; Kolb, B.; Luo, X.; Guo, H.; Jiang, B. Ab Initio Molecular Dynamics Study of Dissociative Chemisorption and Scattering of CO2 on Ni(100): Reactivity, Energy Transfer, Steering Dynamics, and Lattice Effects. *J. Phys. Chem. C* **2017,** *121* (10), 5594.
(44) Lang, N. D.; Kohn, W. Theory of Metal Surfaces: Work Function. *Phys. Rev. B* **1971,** *3* (4), 1215.
(45) Xu, F.; Meng, K.; Cheng, B.; Wang, S.; Xu, J.; Yu, J. Unique S-scheme heterojunctions in self-assembled TiO2/CsPbBr3 hybrids for CO2 photoreduction. *Nat. Commun.* **2020,** *11* (1), 4613.
(46) Guan, D.; Zhong, J.; Xu, H.; Huang, Y.-C.; Hu, Z.; Chen, B.; Zhang, Y.; Ni, M.; Xu, X.; Zhou, W.et al. A universal chemical-induced tensile strain tuning strategy to boost oxygen-evolving electrocatalysis on perovskite oxides. *Applied Physics Reviews* **2022,** *9* (1), 011422.
(47) Wang, J.; Wang, S.-q. Surface properties and work function changes induced by atomic oxygen adsorbed on HfC(1 1 1) surface. *Applied Surface Science* **2015,** *357*, 1046.
(48) Hong, X.; Chan, K.; Tsai, C.; Nørskov, J. K. How Doped MoS2 Breaks Transition-Metal Scaling Relations for CO2 Electrochemical Reduction. *ACS Catal.* **2016,** *6* (7), 4428.
(49) Ju, L.; Tan, X.; Mao, X.; Gu, Y.; Smith, S.; Du, A.; Chen, Z.; Chen, C.; Kou, L. Controllable CO2

electrocatalytic reduction via ferroelectric switching on single atom anchored In2Se3 monolayer. *Nat. Commun.* **2021,** *12* (1), 5128.
(50) Bronsted, J. Acid and Basic Catalysis. *Chemical Reviews* **1928,** *5* (3), 231.
(51) Evans, M.; Polanyi, M. Inertia and driving force of chemical reactions. *Trans. Faraday Soc.* **1938,** *34*, 11.
(52) Varley, J. B.; Hansen, H. A.; Ammitzbøll, N. L.; Grabow, L. C.; Peterson, A. A.; Rossmeisl, J.; Nørskov, J. K. Ni–Fe–S Cubanes in CO2 Reduction Electrocatalysis: A DFT Study. *ACS Catal.* **2013,** *3* (11), 2640.
(53) Kresse, G.; Furthmüller, J. Efficiency of ab-initio total energy calculations for metals and semiconductors using a plane-wave basis set. *Comput. Mater. Sci.* **1996,** *6* (1), 15.
(54) Kresse, G.; Furthmüller, J. Efficient iterative schemes for ab initio total-energy calculations using a plane-wave basis set. *Phys. Rev. B* **1996,** *54* (16), 11169.
(55) Blöchl, P. E. Projector augmented-wave method. *Phys. Rev. B* **1994,** *50* (24), 17953.
(56) Hammer, B.; Hansen, L. B.; Nørskov, J. K. Improved adsorption energetics within density-functional theory using revised Perdew-Burke-Ernzerhof functionals. *Phys. Rev. B* **1999,** *59* (11), 7413.
(57) Grimme, S. Semiempirical GGA-type density functional constructed with a long-range dispersion correction. *J. Comput. Chem.* **2006,** *27* (15), 1787.
(58) Grimme, S.; Antony, J.; Ehrlich, S.; Krieg, H. A consistent and accurate ab initio parametrization of density functional dispersion correction (DFT-D) for the 94 elements H-Pu. *J. Chem. Phys.* **2010,** *132* (15), 154104.
(59) Nørskov, J. K.; Rossmeisl, J.; Logadottir, A.; Lindqvist, L.; Kitchin, J. R.; Bligaard, T.; Jonsson, H. Origin of the overpotential for oxygen reduction at a fuel-cell cathode. *J. Phys. Chem. B* **2004,** *108* (46), 17886.
(60) Mathew, K.; Sundararaman, R.; Letchworth-Weaver, K.; Arias, T.; Hennig, R. G. Implicit solvation model for density-functional study of nanocrystal surfaces and reaction pathways. *J. Chem. Phys.* **2014,** *140* (8), 084106.
(61) Mathew, K.; Kolluru, V. C.; Mula, S.; Steinmann, S. N.; Hennig, R. G. Implicit self-consistent electrolyte model in plane-wave density-functional theory. *J. Chem. Phys.* **2019,** *151* (23), 234101.